SUPPLEMENTARY FILES

RNF217 regulates iron homeostasis through its E3 ubiquitin ligase activity by modulating ferroportin degradation

Li Jiang, Jiaming Wang, Kai Wang, Hao Wang, Qian Wu, Cong Yang, Yingying Yu, Pu Ni, Yueyang Zhong, Zijun Song, Enjun Xie, Ronggui Hu, Junxia Min, and Fudi Wang

This file includes:

Supplemental Methods

Supplemental Table 1-6

Supplemental Figure 1-12

Supplemental Methods

Measurements of serum iron, transferrin saturation (TS), and tissue non-heme iron

Serum iron concentration and TS were measured using a serum iron-unsaturated iron-binding capacity kit (Pointe Scientific, Inc.) in accordance with the manufacturer's instructions. Tissue non-heme iron concentration was measured as previously described[1,2] and are presented as μg iron per gram wet weight of tissue.

Histochemistry

Tissue iron was visualized in paraffin-embedded sections using Perls' Prussian blue staining or enhanced DAB staining, and tissue FPN protein was visualized using FPN immunohistochemistry (IHC), all of which were performed as previously described.[1]

Microscope

Microcopy images were captured using an Olympus BX61 microscope equipped with a UPlanSApo 20×/0.75 or UPlanSApo 40×/0.90 objective, an Olympus DP26 camera and cellSens Standard imaging software (Olympus).

Real-time PCR analysis

Total RNA was extracted using TRIzol reagent, and then reverse-transcribed into cDNA using the PrimeScript RT kit (Takara). Real-time PCR (RT-PCR) was then performed using the two-step real-time quantitative RT-PCR method (Bio-Rad) with the primers listed in Supplementary Table S4. For *Fpn* mRNA levels detection, all transcripts of *Fpn* are covered in the liver, spleen, BMDMs and enterocytes mRNA quantification by using *Fpn* qPCR primers (general primers), and specific qPCR primers for *Fpn1a, Fpn1b*.

Mouse primary mouse macrophage cultures

BMDMs were cultured and treated as described previously.[1] Unless stated otherwise, cells were incubated with FAC (100 μg) for 20 h to increase endogenous FPN expression.

Confocal immunofluorescence microscopy

For 5-hmC immunofluorescence staining of BMDMs, cells were fixed in 4% paraformaldehyde for 15 min, washed three times with phosphate-buffered saline (PBS), and blocked in blocking solution (PBS containing 5% fetal bovine serum and 10.5% Tween 20) for 2 h at room temperature (20–25°C). The primary antibody against 5-hydroxymethylcytosine (1:100, Active Motif) was diluted in blocking solution and then

incubated with the cells overnight at 4°C. The cells were then washed three times in PBS and incubated for 2 h at room temperature with Cy3-labeled goat anti-rabbit IgG (H+L) (1:1,000, Beyotime) diluted in blocking solution. The cells were then washed three times in PBS and imaged as described previously.[3] For exogenous FPN and RNF217 staining, HeLa cells were transfected with the indicated plasmids, cultured for at least 24 h, treated with FAC (100 μg) for 12 h, fixed with 4% paraformaldehyde, and then stained with anti-Flag and anti-Myc primary antibodies (1:1,000, Cell Signaling Technology), followed by FITC-labeled goat anti-mouse IgG (H+L) and Cy3-labeled goat anti-rabbit IgG (H+L) (1:1,000, Beyotime) secondary antibodies. Confocal images were acquired under a Zeiss LSM880 confocal laser scanning microscope equipped with a 63× oil-immersion objective (1.4 NA DIC). The dual- and triple-labeled cells were imaged using separate channels in a sequential setting. Green fluorescence was excited using an Ar 488-nm laser, red fluorescence was excited using a DPSS KL561-nm laser, and far-red fluorescence was excited using a HeNe 633-nm laser. All signals collected using gallium arsenide phosphide (GaAsP) and photomultiplier tube (PMT) detectors were merged, and separate images for each channel were retained. The images were taken at 2× zoom and processed using Zeiss Zen2.3 (black edition) software.

TET activity assay

Mouse BMDMs were incubated with the indicated concentration of FAC for 12 h, and nuclear protein extracts were prepared as described previously.[4] TET activity was measured in the fresh nuclear protein extracts using the fluorometric Epigenase 5mC Hydroxylase TET Activity/Inhibition Assay Kit (EpiGentek).

Detection of 5-hmC

5-hmC modification of the *Rnf217* promoter was assayed using the glucosylation-mediated restriction enzyme sensitive qPCR (GRES-qPCR) method.[5] The EpiMark kit (NEB) was used to quantify the relative levels of 5-hmC at select loci in FAC-treated BMDMs and small intestinal villus enterocytes obtained from HID-treated mice, in accordance with the manufacturer's instructions. In brief, 10 μg of genomic DNA was used; half was treated with T4-phage βGT for 12–16 h at 37°C; the other half was untreated. Both the βGT-treated and untreated samples were then divided into three microtubes and digested with MspI, HpaII, or no enzyme for 12–16 h at 37°C. The samples were then treated with proteinase K for 10 min at 40°C, diluted with water to a final volume of 100 μl, and heated at 95°C for 5 min. Quantitative PCR was then performed with approximately 0.8 μg of DNA in 5 μl using a LightCycler 480 PCR machine (Roche); the primers used for these experiments are listed in Supplementary Table S5. Relative enrichment of 5-hmC was then calculated using the formulas provided by NEB.

Bisulfite Sanger sequencing

BMDMs were isolated from *Tet1*$^{+/+}$ and *Tet1*$^{-/-}$ mice, treated with FAC for 12 h, and analyzed for *Rnf217* promoter methylation. To analyze the methylation status of the *Rnf217* promoter, 0.2 μg of genomic DNA was subjected to sodium bisulfite conversion using the EZ DNA Methylation-Gold kit (Zymo Research). Bisulfite-treated DNA was then subjected to PCR amplification using the primers listed in Supplementary Table S6. The PCR products were purified using the Gel Extraction Kit (Qiagen) and cloned into the pMD19-T vector (Takara). Individual clones were sequenced using standard Sanger sequencing, and the data were analyzed using the online tool BISMA (http://services.ibc.uni-stuttgart.de/BDPC/BISMA/) as described previously.[6]

Flow cytometry analysis

CD11b, F4/80, and Calcein fluorescence were measured in splenic macrophages and BMDMs using flow cytometry as previously described.[7] In brief, the cells were incubated either with or without the high-affinity iron chelator 2,2'-bipyridyl, washed, and then loaded with Calcein-AM (final concentration: 0.5 mM) for 10 min at 37°C. After washing, the macrophage population was verified by staining with anti-CD11b (BioLegend) and F4/80 (BioLegend) for 30 min at 4°C. Flow cytometry was performed using an LSR Fortessa cell analyzer (BD Biosciences, San Jose, CA).

RNA-seq analysis

For the SID- and LID-fed groups, 3-week-old male C57B/6J mice were fed the standard-iron diet or low-iron diet, respectively, for 9 weeks; for the HID-fed group, 3-week-old male C57B/6J mice were fed the standard-iron diet for 3 weeks followed by the high-iron diet for 6 weeks. Total hepatic RNA was then isolated from 3 mice per group, and RNA-seq libraries were generated using the TruSeq RNA Sample Preparation Kit (Illumina). RNA-seq reads were mapped to the mouse reference genome using TopHat. Only uniquely aligned reads were used for gene and exon quantification. The Cufflinks tool was used to quantify isoform expression.[8,9]

DNA methylation sequencing

Genomic DNA from the livers of C57B/6J mice was extracted and purified using the Qiagen DNeasy Kit, and DNA methylation sequencing was performed as previously described.[10,11] CpG methylation status across the genome was characterized using methylation-sensitive HpaII and the methylation-insensitive isoschizomer MspI; both enzymes target the same CCGG sequence, and sequencing read counts mapped to HpaII and MspI cutting sites provide a quantitative digital measure of CpG methylation within genomic CCGG sites. For sequencing read alignment, a set of possible 17- and 18-bp

tags was created from all CCGG sites in the *Mus musculus* genome assembly (mm9, downloaded from the UCSC genome browser at http://genome.ucsc.edu/). The locations of the CCGG sites were annotated as the gene promoter (-2000 to -1 bp), coding sequence (CDS), exon, intron, 5' UTR, 3' UTR, or intergenic region. Differentially methylated sites were analyzed using a one-way ANOVA (R package) and mapped to signaling pathways using the KEGG pathway mapping tool (http://www.genome.jp/kegg/tool/map_pathway1.html).

Supplementary Table S1. Differentially expressed E3 ligase genes from Tet1 knockout systems.

Gene	Tet1 bound	Expression Tested	Molecular Function	Reference(s)
Amfr	Yes	Tet1-depleted ES cells	E3 ubiquitin-protein ligase that mediates the polyubiquitination of lysine and cysteine residues on target proteins for proteasomal degradation.	[12]
Asb2	Unknown	Tet1-depleted ES cells; Tet1-depleted cancer cells	Substrate-recognition component of a SCF-like ECS E3 ubiquitin-protein ligase complex which mediates the ubiquitination and subsequent proteasomal degradation of target proteins.	[13]
Clu	Yes	Tet1-depleted ES cells	Binding to cell surface receptors triggers internalization of the chaperone-client complex and subsequent lysosomal or proteasomal degradation.	[12]
Dyrk2	Yes	Tet1-depleted ES cells	Serine/threonine-protein kinase functions in part via its role in ubiquitin-dependent proteasomal protein degradation.	[12]
Fbxo15	Yes	Tet1-depleted ES cells	Substrate-recognition component of the SCF type E3 ubiquitin ligase complex.	[12]
Klhl10	Yes	Tet1-depleted ES cells	May be a substrate-specific adapter of a CUL3-based E3 ubiquitin-protein ligase complex which mediates the ubiquitination and subsequent proteasomal degradation of target proteins during spermatogenesis.	[12]
Klhl42	Yes	Tet1-depleted ES cells	Substrate-specific adapter of a BCR E3 ubiquitin-protein ligase complex, mediates the ubiquitination and subsequent degradation of KATNA1.	[12]
Nf2	Yes	Tet1-depleted ES cells	Suppresses cell proliferation and tumorigenesis by inhibiting the CUL4A-RBX1-DDB1-VprBP/DCAF1 E3 ubiquitin-protein ligase complex.	[12]
Pdzrn3	Yes	Tet1-depleted ES cells	E3 ubiquitin-protein ligase mediates the ubiquitination of MUSK, promoting its endocytosis and lysosomal degradation.	[12]

Rnf11	Yes	Tet1-depleted ES cells	Essential component of a ubiquitin-editing protein complex, comprising also TNFAIP3, ITCH and TAX1BP1, that ensures the transient nature of inflammatory signaling pathways.	[12]
Rnf128	Yes	Tet1-depleted ES cells	E3 ubiquitin-protein ligase that catalyzes Lys-48- and Lys-63-linked polyubiquitin chains formation.	[12]
Rnf138	Yes	Tet1-depleted ES cells	E3 ubiquitin-protein ligase involved in DNA damage response by promoting DNA resection and homologous recombination.	[12]
Rnf217	Yes	Tet1-depleted ES cells	E3 ubiquitin-protein ligase which accepts ubiquitin from E2 ubiquitin-conjugating enzymes in the form of a thioester and then directly transfers the ubiquitin to targeted substrates.	[12]
Socs5	Yes	Tet1-depleted ES cells	May be a substrate-recognition component of a SCF-like ECS E3 ubiquitin-protein ligase complex which mediates the ubiquitination and subsequent proteasomal degradation of target proteins.	[12]
Tnip1	Yes	Tet1-depleted ES cells	Binding to polyubiquitin.	[12]
Trim2	Yes	Tet1-depleted ES cells	UBE2D1-dependent E3 ubiquitin-protein ligase that mediates the ubiquitination of NEFL and of phosphorylated BCL2L11.	[12]
Trim25	Unknown	Tet1-depleted ES cells; Tet1-depleted cancer cells	Functions as a ubiquitin E3 ligase and as an ISG15 E3 ligase.	[13,14]
Trim68	Yes	Tet1-depleted ES cells	Functions as a ubiquitin E3 ligase. Acts as a coactivator of androgen receptor (AR) depending on its ubiquitin ligase activity.	[12]
Ube2l6	Yes	Tet1-depleted ES cells	Ubiquitin conjugating enzyme H8, identified in a two-hybrid screen through specific interaction with E6AP (E3) ubiquitin protein ligase in the E6-dependent ubiquitination of TP53	[12]

Vprbp (Dcaf1)	Unknown	Unknown	Acts both as a substrate recognition component of E3 ubiquitin-protein ligase complexes and as an atypical serine/threonine-protein kinase.	[15]
Wdtc1	yes	Tet1-depleted ES cells	May function as a substrate receptor for CUL4-DDB1 E3 ubiquitin-protein ligase complex.	[12]
Wsb2	Unknown	Tet1-depleted ES cells; Tet1-depleted cancer cells	May be a substrate-recognition component of a SCF-like ECS E3 ubiquitin ligase complex which mediates the ubiquitination and subsequent proteasomal degradation of target proteins.	[13,14]

Supplementary Table S2. Blood parameters of 8-week-old *Rnf217*$^{Villin/Villin}$ mice or *Rnf217*$^{Lysm/Lysm}$ mice, and their corresponding control (*Rnf217*$^{flox/flox}$) littermates.

Hematology	***Rnf217*$^{flox/flox}$ (n=5)**	***Rnf217*$^{Villin/Villin}$ (n=5)**	***P-value***	***Rnf217*$^{flox/flox}$ (n=7)**	***Rnf217*$^{Lysm/Lysm}$ (n=6)**	***P-value***
RBCs, 10^{12}/L	8.95±0.65	9.36±0.22	0.2623	8.87±0.24	8.83±0.17	0.7760
Hb, g/L	13.52±0.63	14.04±0.76	0.3214	13.43±0.37	12.88±0.51	0.0663
Hct, %	44.24±2.48	46.16±2.55	0.3126	45.43±1.28	43.93±1.71	0.1266
MCV, fL	49.50±1.13	49.28±1.84	0.8433	51.21±1.18	49.77±1.87	0.1484

Hb, hemoglobin; Hct, hematocrit; MCV, mean corpuscular volume; RBCs, red blood cells.

Supplementary Table S3. Sequences of the primers used for PCR-based genotyping

Primer name	Primer sequence (5'-3')
Tet1-C	CAGTAGTATTTTGCCTGCCTGCAT
Tet1-F	CATCCTAAATAACCCAACCACCAA
Tet1-R	TTCCCTAAGGAGTTTACTGCAACG
Rnf217-flox-P5	ATCCAGGGTCTCCAGCAATT
Rnf217-flox-P6	CTGCGTTCCCCTGTTTGGTT
Lysm-Cre-F	CTTGGGCTGCCAGAATTTCTC
Lysm-Cre-R	CGCGCCTGAAGATATAGAAGA
Lysm-Cre-wt	TTACAGTCGGCCAGGCTGAC
pVillin-Cre-F	CAAGCCTGGCTCGACGGCC
pVillin-Cre-R	CGCGAACATCTTCAGGTTCT

142 **Supplementary Table S4**. Sequences of the primers used for RT-PCR analyses

143

Gene name	Forward primer (5'-3')	Reverse primer (5'-3')
Fpn	GTCGGCCAGATTATGACATTTG	ATTCCAACCGGAAATAAAACCA
Fpn1a	AAAGAAGACCCCGTGACAGC	TCCCCGTGTTTGTTCTGATG
Fpn1b	GCCGGTTGGAGTTTCAATGT	TCCCCGTGTTTGTTCTGATG
Hamp1	GCACCACCTATCTCCATCAACA	TTCTTCCCCGTGCAAAGG
Tfr1	TGGCTGAAACGGAGGAGACAGA	TGGCTCAGCTGCTTGATGGTGT
Fth	AAGATGGGTGCCCCTGAAG	CCAGGGTGTGCTTGTCAAAGA
Gapdh	ATCATCCCTGCATCCACT	ATCCACGACGGACACATT
Asb2	TCCAGGGAGACTCCACTTTACA	CAATATCCTCACCGCCTCCG
Trim25	CGTACAACCTTCGAAGAAGACCA	TTAGGTGAGAAGTGGGAGGGA
Wsb2	GACTGTAGCATGCTGTGCTCT	CGGATTAGTGTGTAGGACCGC
Vprbp	GAGAAGCGGCGGAGCC	AGTGAGCTCAGCTTTGGAGTC
Amfr	GCCCAGTACCTGCTGTCG	ACAGCAAGCAGTATTCACCAGA
Klhl42	AATCCCATCACCAACGAGTGG	AAGCTTTGAATTGACAGCCACAA
Clu	AGAGCAGGAGGTCTCTGACAA	GACGGCGTTCTGAATCTCCTTA
Rnf128	TTTGGTGCGCATCCTAACCT	TCTAAAAGCCACGGGTCCAC
Rnf217	GCGAGGAGTGCCTCAAAATCT	AAACACTCTGTGACTGGGCAT
Rnf11	ATGACCCTGGAAGAGATGGATCA	GGGTCCCCATAAACAAAGTCCA
Socs5	CGTAGTGGGAGCTTACTCGC	ATCAGCTTCCCGCTTCAGAC
Dyrk2	GCCAGCAACGCTACCACTA	TGTTGAGGTGGAGGTGGTCA
Trim68	AAGCCCACAGTGTTGTACCC	CCAGAGCCTGCTGGAGTTTC
Pdzrn3	GAAGAAGTTCACCGAGTACAGC	TCAGGCTTTTGGTCTCTTCTCC
Ube2l6	TTGTGTGGCACATGCTCCT	TGGGGAAATCAATCCGCACTT
Klhl10	GCCCACAAGAACATCCTCTGTA	AGTGTTGTTCCAGCCACTTGT
Fbxo15	AATGGAGGAGTCGGAATTGGAG	TGCTTCGTGACAGATGAGCC
Tnip1	CCTCGTGCATTCTCGGATGA	TTCCATGAGGGTGGCTCAAC
Trim2	TTTGGTAGCCGAGGAAACGG	ATTCACAGCTGCAAAGTGGG
Nf2	GGCCTGGCTCAAAATGGACA	TTGGCCAGGAAGTGAAAGGT
Rnf138	GTCAGGAGGTGCTCAAGACG	TCTCTCATTGCAGTCAGGAAACAT
Wdtc1	ATGGGCTCCTGAAGTTGCTC	CCAGGTCCACAAGACAAGCA

Supplementary Table S5. Sequences of the primers used for PCR-based 5hmC detection

Primer pair	Forward primer (5'-3')	Reverse primer (5'-3')
5hmC-*mRnf217*-P1	CACCTCTCGGTGACGCC	AGGAGACGGTCAGCCCC
5hmC-*mRnf217*-P2	GCGACGTGCATGCGG	TCGAGGACTCCGAGGGC
5hmC-*mRnf217*-P3	GAGTCCTCGAGGCGGTG	GACGCCCCAAGCGCC
5hmC-*mRnf217*-P4	GGGGCTGACCGTCTCCT	GCATGCACGTCGCGG
5hmC-*mRnf217*-P5	GGCGCTTGGGGCGTC	GGCTCCGCTCCACTCG
5hmC-*mRnf217*-P6	GGCGCTTGGGGCGTC	TCTGCTCCTCGCCCATC

Supplementary Table S6. Sequences of the primer pairs used for PCR-based bisulfite sequencing.

Primer name	Primer sequence (5'-3')
BS-*mRnf217*-P1-F	TATTGAGTAGAGGAAAAGTAGTAAATGTTA
BS-*mRnf217*-P1-R	ACCCCAACCAAATACTTAAAC
BS-*mRnf217*-P2-F	TTATTTAAAGTAGAGTATTAAGGGG
BS-*mRnf217*-P2-R	CAATAACTAATATCCCTAAAAAAAA

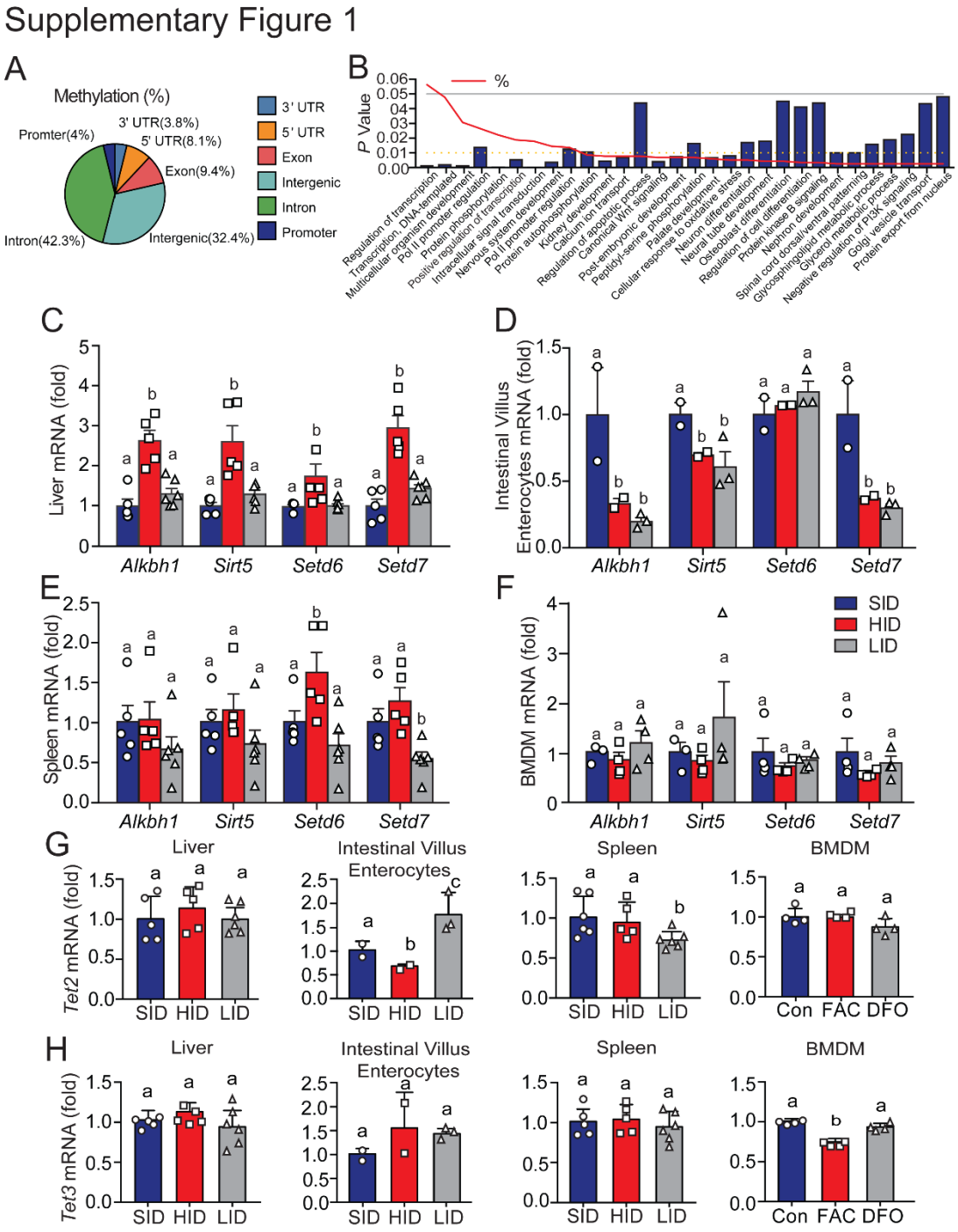

Supplementary Figure S1. High iron induces global methylation change and differential expression of genes involved in epigenetic modification. A. Distribution of single CpG methylation levels across the indicated genomic elements in the liver of mice fed a high-iron diet (HID) (pooled data from 3 mice). B. Gene Ontology (GO) analysis of all genes with differentially methylated promoter regions measured in the liver of HID-fed mice, ranked from the most common to the least common (n=3 mice/group). C-F. RT-PCR analysis of relative mRNA levels in the indicated tissues

and cells of mice fed a standard-iron diet (SID), high-iron diet (HID), or low-iron diet (LID) (for liver and spleen, n=5-6 mice/group; for enterocytes, every spot/box represent 2-3 mice, n=5-6 mice/group; for BMDM, n= 3-4 per group); each gene was normalized to the respective SID-fed group; G-H. RT-PCR analysis of *Tet2* (G), and *Tet3* (H) mRNA measured in the indicated tissues and cells of mice fed the indicated diets (for the liver and spleen, n=5-6 mice/group; for enterocytes, every spot/box represents 2-3 mice, n=5-6 mice/group; for BMDM, n= 3-4 per group). Groups labeled without a common letter were significantly different ($P<0.05$), one-way ANOVA.

Supplementary Figure 2

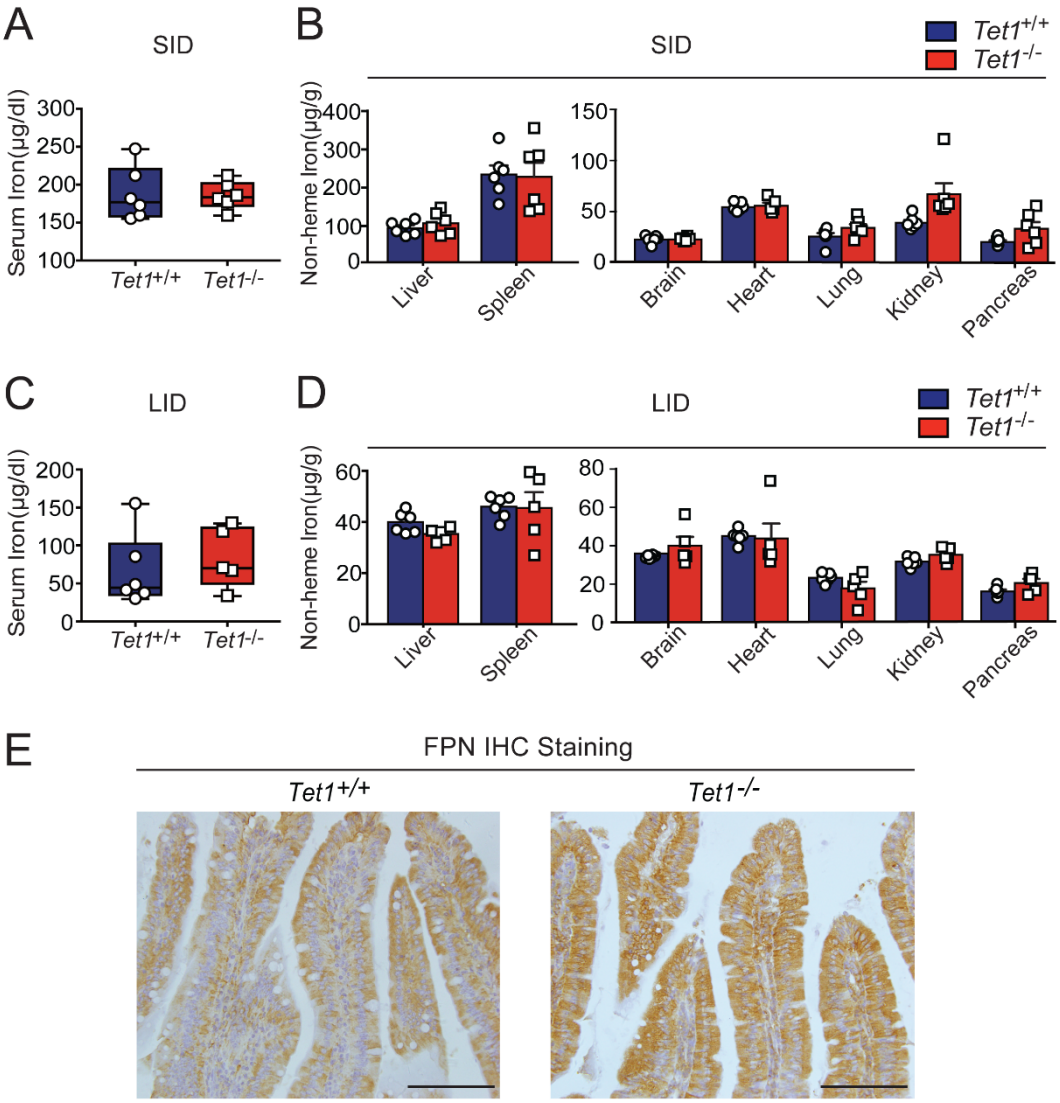

Supplementary Figure S2. *Tet1* knockout mice have normal iron status when fed either a standard-iron diet or a low-iron diet. A-D. Serum iron levels (A and C) and tissue non-heme iron concentration (B and D) were measured in 8-week-old *Tet1*$^{+/+}$ and *Tet1*$^{-/-}$ mice fed either a standard-iron diet (SID; A and B) or a low-iron diet (LID; C and D) for 5 weeks (n=5-6 per group); E. Higher magnification of FPN immunohistochemistry (IHC) in duodenum (n=3 per group). The scale bars in E represent 100 μm. All group differences were not significant (P>0.05, Student's t-test).

Supplementary Figure 3

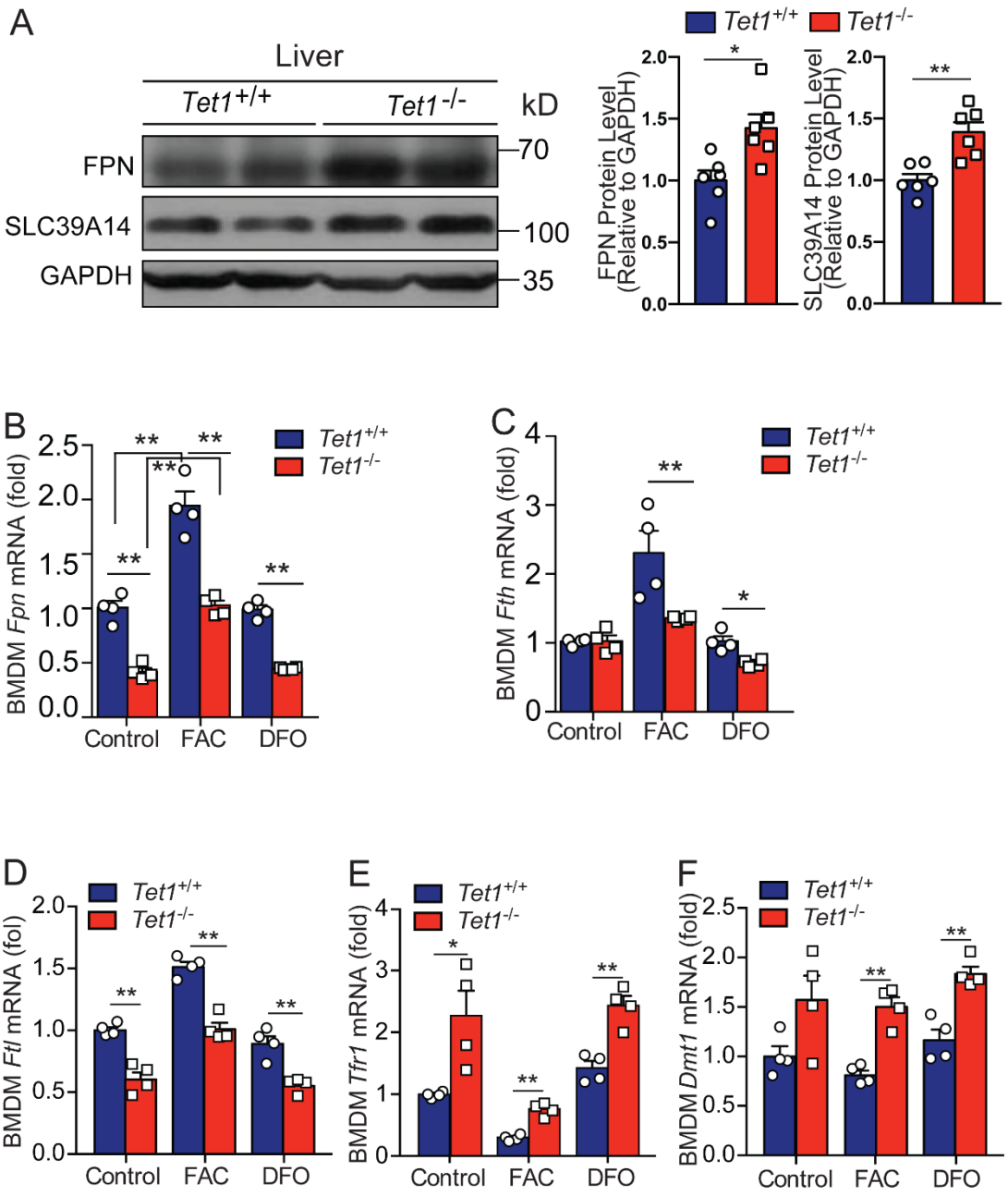

Supplementary Figure S3. Loss of *Tet1* alters the expression of iron-regulatory genes. A. Western blot analysis and summary of FPN and SLC39A14 protein levels measured in liver from iron dextran–injected *Tet1*$^{+/+}$ and *Tet1*$^{-/-}$ mice (n=6 mice/group). B-F. RT-PCR analysis of relative *Fpn* (B), *Fth* (C), *Ftl* (D), *Tfr1* (E), and *Dmt1* (F) mRNA levels measured in untreated (control), FAC-treated, and DFO-treated BMDMs isolated from *Tet1*$^{+/+}$ and *Tet1*$^{-/-}$ mice, normalized to the respective untreated *Tet1*$^{+/+}$ cells (n=4 per group). **P*<0.05 and ***P*<0.01, Student's *t*-test.

Supplementary Figure 4

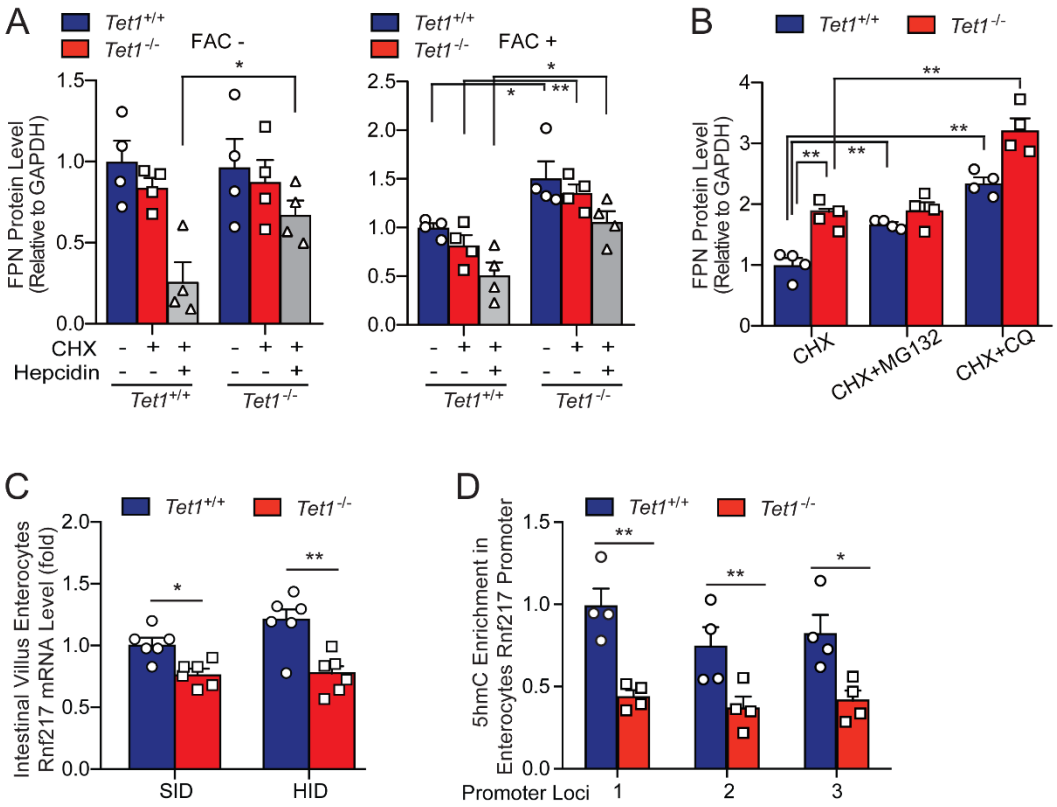

Supplementary Figure S4. Downregulation of *Rnf217* gene expression and promoter 5hmC enrichment in the duodenum of *Tet1*$^{-/-}$ mice. A and B. Quantitative analyses of FPN in BMDMs obtained from *Tet1*$^{+/+}$ and *Tet1*$^{-/-}$ mice treated as indicated (n=4 mice/group). C. Relative *Rnf217* mRNA levels were measured in the duodenal enterocytes of SID- and HID-fed *Tet1*$^{+/+}$ and *Tet1*$^{-/-}$ mice, normalized to the SID-fed *Tet1*$^{+/+}$ group (n=5-6 mice/group). D. Relative enrichment of 5-hmC at three loci in the *Rnf217* promoter was measured in the duodenal enterocytes of HID-fed *Tet1*$^{+/+}$ and *Tet1*$^{-/-}$ mice (n=3 mice/group). **P*<0.05 and ***P*<0.01, Student's *t*-test.

Supplementary Figure 5

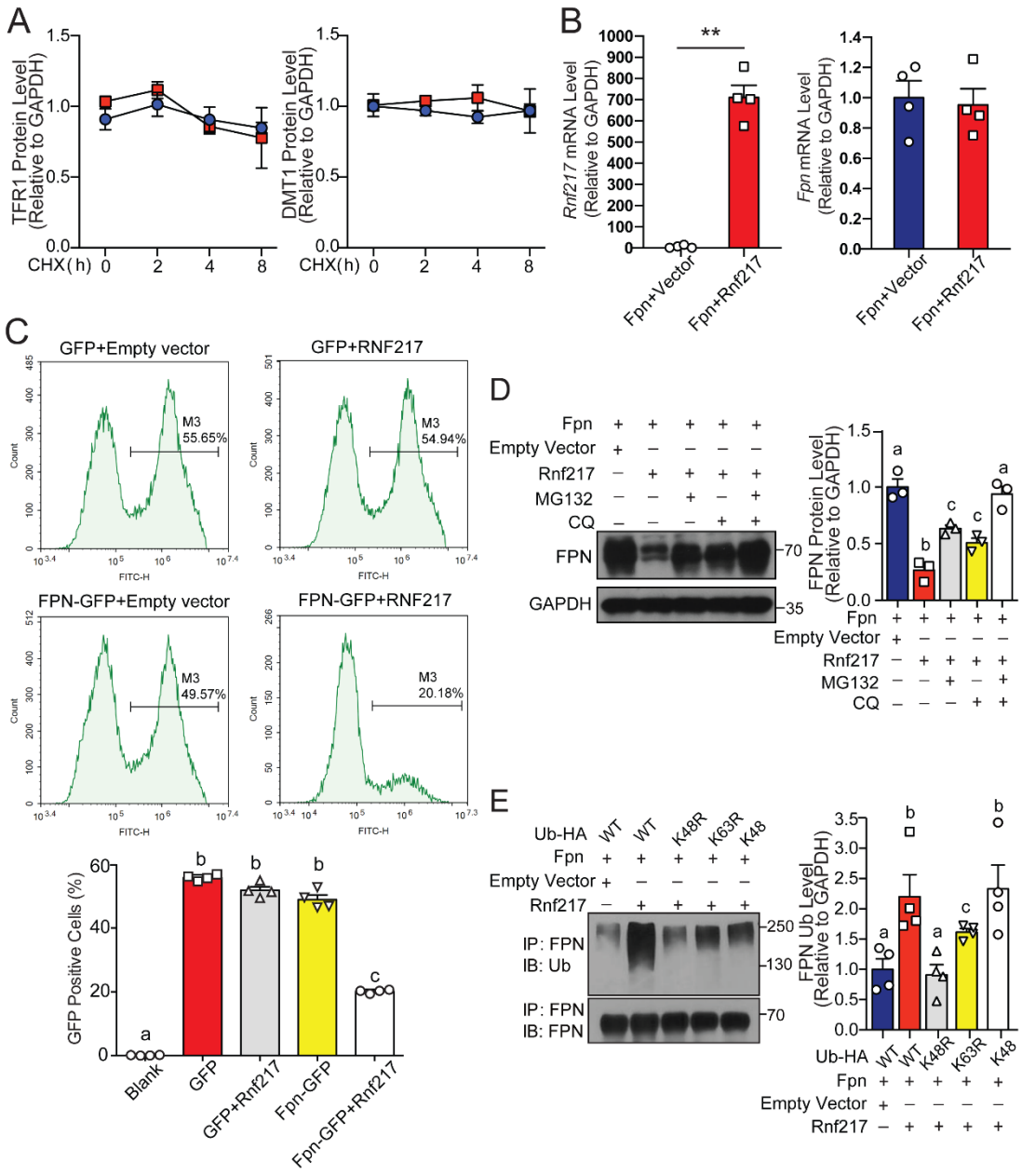

Supplementary Figure S5. Rnf217 specifically regulates proteasome-dependent FPN degradation. A. Quantitative analyses of TFR1 and DMT1 in HEK293T cells transfected with FPN and RNF217 and treated with cycloheximide (CHX) for the indicated times (n=4 experiments/group). B. *Rnf217* and *Fpn* mRNA was measured in HEK293T cells transfected with FPN together with an empty vector or RNF217 (n=4 experiments/group). C. HeLa cells transfected with the indicated constructs were analyzed using FACS analysis (n=4 experiments each). D. HEK293T cells were transfected with Fpn-Myc and either an empty vector or Rnf217-Flag, and then treated

with CHX (75 μM) for 2 hours, followed by MG132 (10 μM) and/or CQ (400 μM) for an additional 4 hours. FPN was then measured using western blot analysis (n=3 experiments/group). E. HEK293T cells were transfected with Fpn-Myc and either an empty vector or Rnf217-Flag, together with an HA-tagged wild-type (WT) or mutant ubiquitin (Ub); cell lysates were then immunoprecipitated using an anti-FPN antibody and immunoblotted using an anti-poly-Ub antibody to detect the ubiquitination level of FPN (n=4 experiments/group). In B, $^{**}P<0.01$ (Student's *t*-test); in C-E, groups labeled without a common letter were significantly different ($P<0.05$; one-way ANOVA).

Supplementary Figure 6

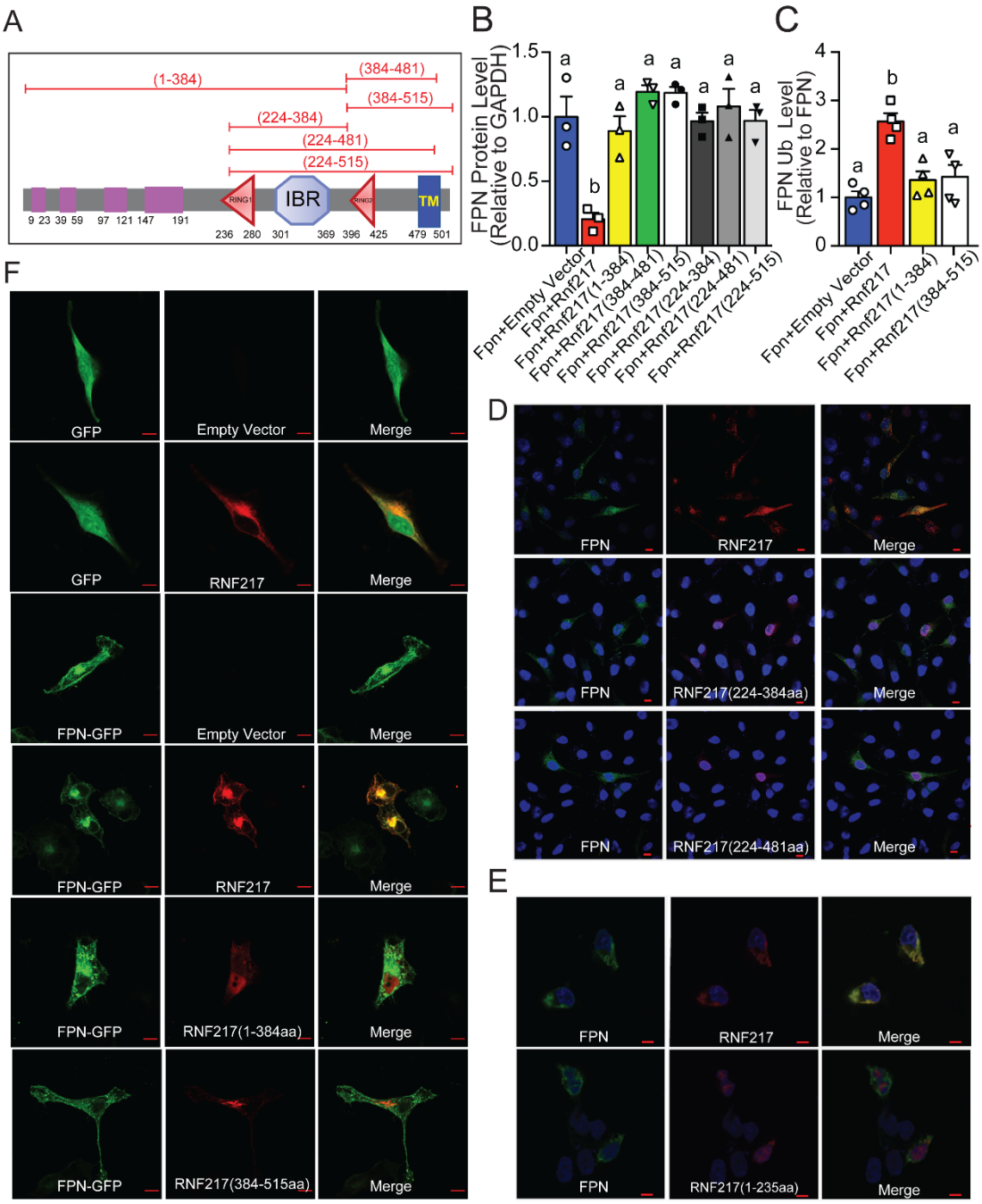

Supplementary Figure S6. Truncations in RNF217 reduce RNF217-mediated FPN degradation and the colocalization between RNF217 and FPN. A. Schematic diagram showing the putative functional domains in the RNF217 protein, with the various truncated forms of RNF217 used in this study indicated above. B and C. Quantitative analyses for FPN (B) and FPN Ub (C) levels in HEK293T cells transfected with FPN and either an empty vector or the indicated RNF217 constructs (n=3-4 experiments/group). D. Example immunofluorescence images of HeLa cells transfected with FPN and either full-length RNF217 or the indicated truncated forms of RNF217;

the nuclei were counterstained with DAPI. E. Example immunofluorescence images of HEK293T cells co-transfected with FPN and either full-length RNF217 or the indicated mutant RNF217; the nuclei were counterstained with DAPI. F. Example immunofluorescence images of HeLa cells transfected with GFP-construct or FPN-GFP and either full-length RNF217 or the indicated truncated forms of RNF217. The scale bars in D, E, and F represent 10 μm. In B-C, groups labeled without a common letter were significantly different ($P<0.05$; one-way ANOVA).

Supplementary Figure 7

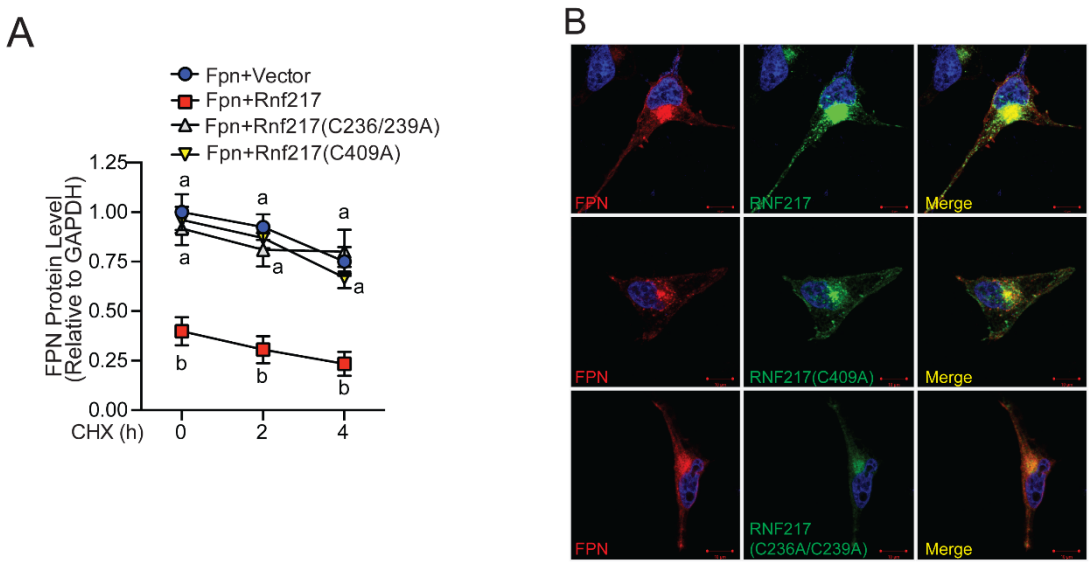

Supplementary Figure S7. Mutations in RNF217 reduce RNF217-mediated FPN degradation. A. Quantitative analyses of FPN measured in HEK293T cells transfected with FPN together with an empty vector of the indicated RNF217 constructs (n=3 experiments/group). B. Example immunofluorescence images of HeLa cells transfected with FPN and the indicated RNF217 constructs; the nuclei were counterstained with DAPI. In A, groups labeled without a common letter were significantly different (P<0.05; (one-way ANOVA). The scale bars in B represent 10 μm.

Supplementary Figure 8

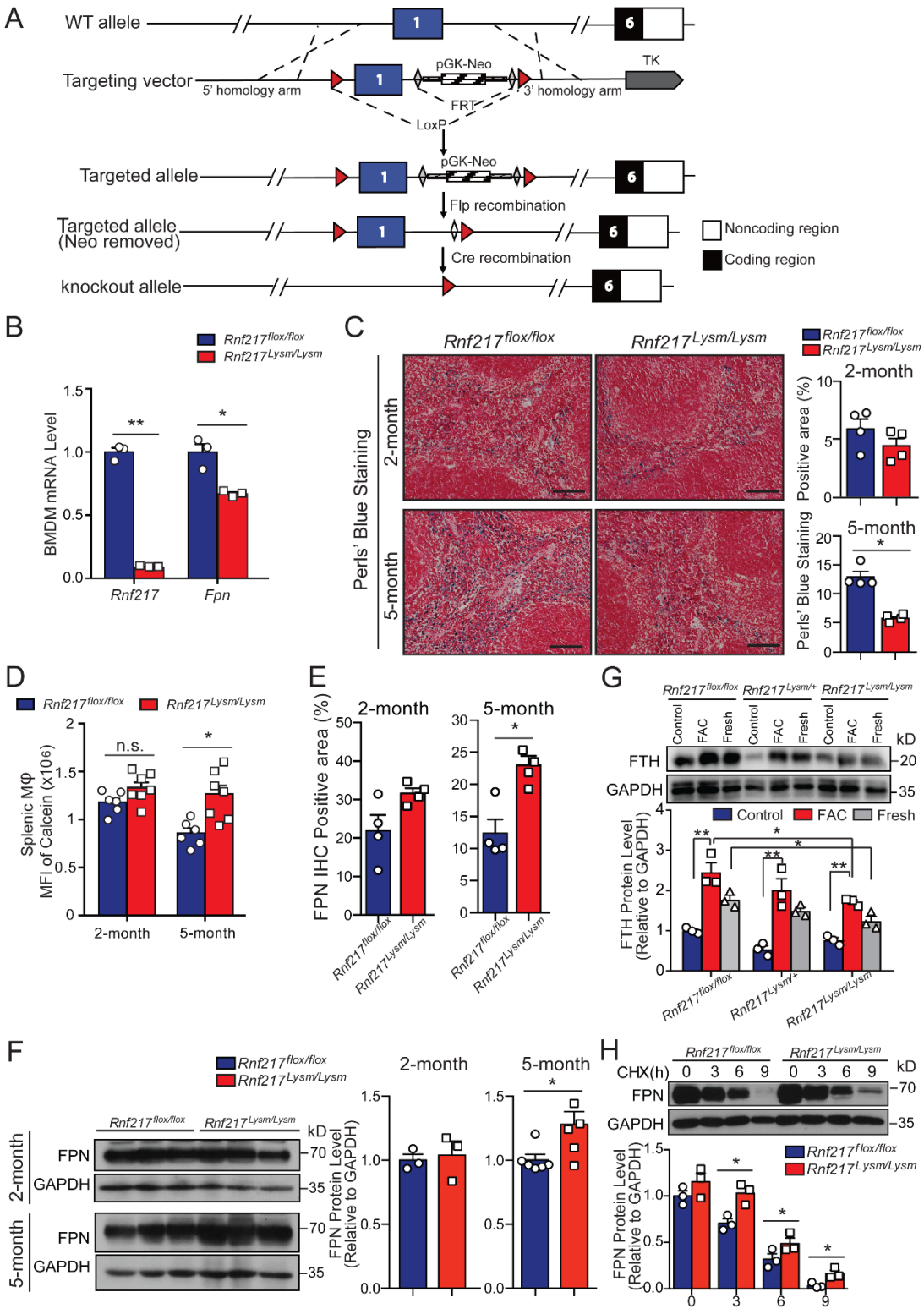

Supplementary Figure S8. Macrophage-specific *Rnf217* knockout mice presented with phenotypes of increased iron exportation and attenuated FPN degradation in macrophages. A. Schematic diagram depicting the targeting strategy used to generate the conditional *Rnf217* knockout (*Rnf217*^{flox}) allele. Exons 1 and 6 are indicated. B. RT-PCR analysis of *Rnf217* and *Fpn* mRNA measured in BMDMs obtained from control (*Rnf217*$^{flox/flox}$) and *Rnf217*$^{Lysm/Lysm}$ mice (n=3 mice/group). C. Perl's Prussian blue staining and quantification of spleen sections prepared from 2-month-old and 5-month-old *Rnf217*$^{flox/flox}$ and *Rnf217*$^{Lysm/Lysm}$ mice (n=4 mice/group). D. Splenic macrophages obtained from *Rnf217*$^{flox/flox}$ and *Rnf217*$^{Lysm/Lysm}$ mice at the indicated ages were loaded with the iron-sensitive fluorophore Calcein-AM and analyzed using flow cytometry (n=6-7 mice/group). E. FPN-positive staining area was quantified (n=4 mice/group). F. Western blot analysis and quantification of FPN measured in spleen samples prepared from *Rnf217*$^{flox/flox}$ and *Rnf217*$^{Lysm/Lysm}$ mice at the indicated ages (n=3-6 mice/group). G. The indicated BMDMs were incubated overnight with FAC (100 μM), washed, and then incubated in fresh medium for 12 hours. Ferritin H (FtH) protein was then measured using western blot analysis and quantified (n=3 experiments/group). H. The indicated BMDMs were incubated overnight with FAC (100 μM) and then treated with CHX (75 μM) for the indicated times, after which FPN was measured using western blot analysis and quantified (n=3 experiments/group). The scale bars in C represent 100 μm. **P*<0.05 and ***P*<0.01 (Student's *t*-test).

Supplementary Figure 9

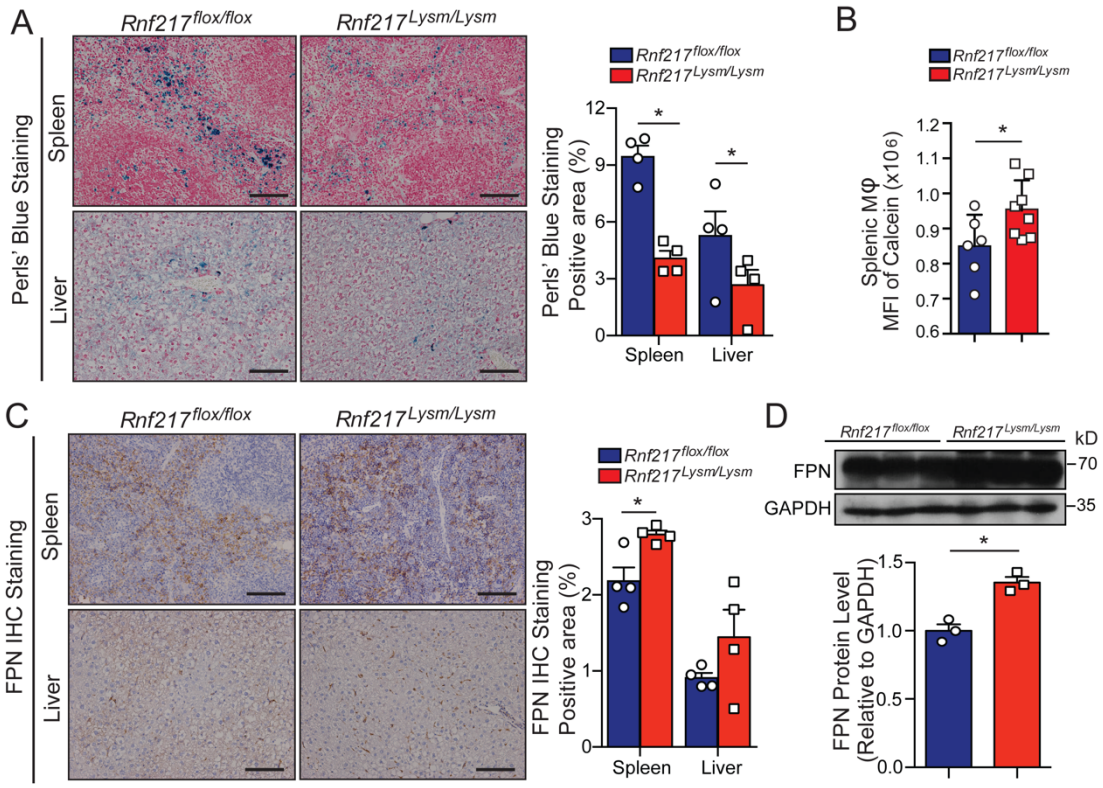

Supplementary Figure S9. Macrophage-specific *Rnf217* knockout mice had altered response to iron overload. A. *Rnf217*$^{flox/flox}$ and *Rnf217*$^{Lysm/Lysm}$ mice were fed a high-iron diet for 6 weeks followed by a low-iron diet for 5 weeks, after which liver and spleen sections were prepared from the mice and stained with Perl's Prussian blue and quantified (n=4 mice/group). B. Summary of mean fluorescence intensity (MFI) measured in Calcein-loaded splenic macrophages obtained from A (n=6-8 mice/group). C. FPN immunohistochemical staining and quantification analysis of spleen sections prepared from A (n=4 mice/group). D. Western blot analysis and quantification of FPN in spleen samples prepared from A (n=3 mice/group). The scale bars in A and C represent 100 μm. **P*<0.05 and ***P*<0.01 (Student's *t*-test).

Supplementary Figure 10

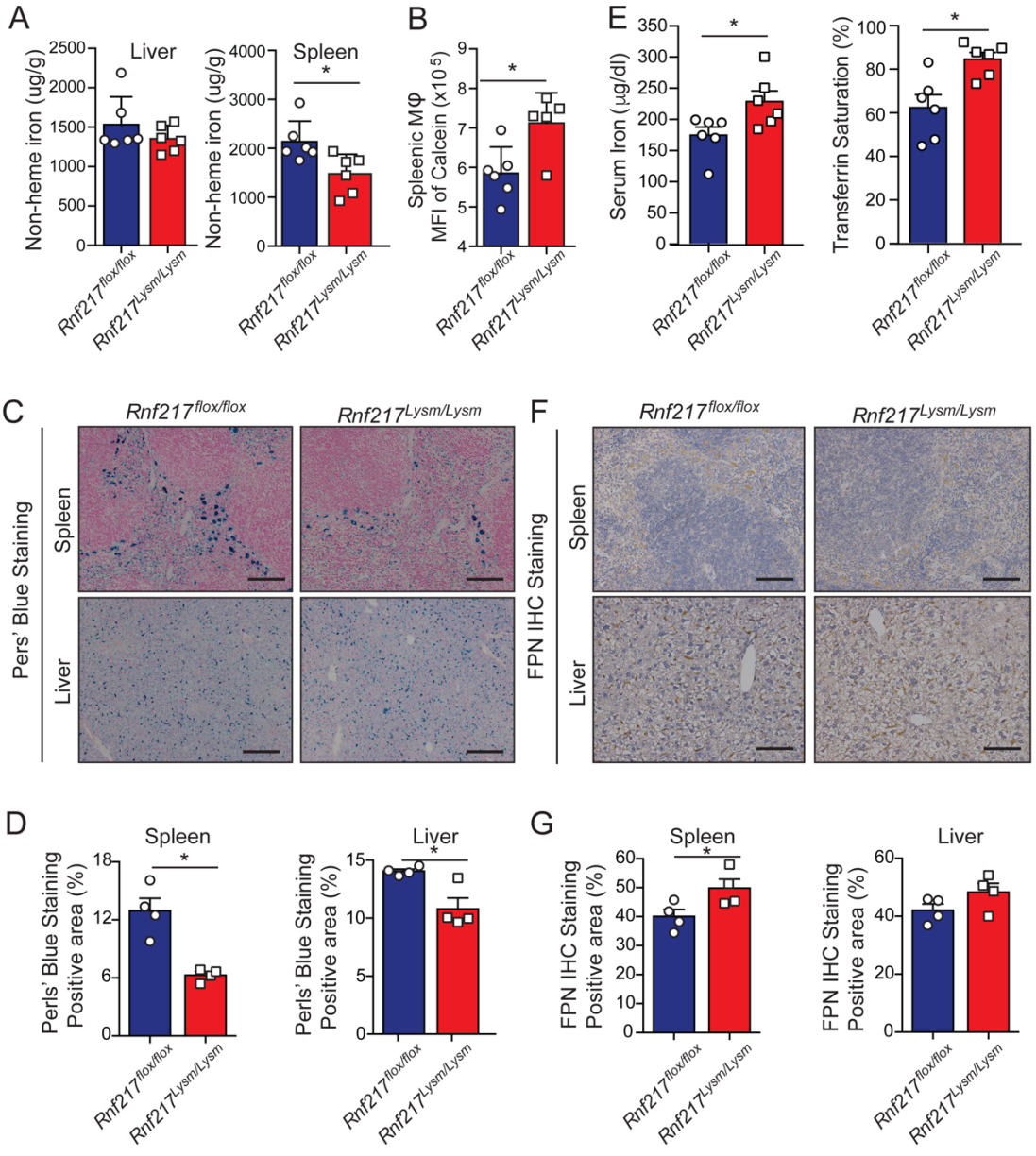

Supplementary Figure S10. Iron dextran facilitates iron export from macrophages in *Rnf217*$^{Lysm/Lysm}$ mice. A. Non-heme iron levels were measured in the liver and spleen of *Rnf217*$^{flox/flox}$ and *Rnf217*$^{Lysm/Lysm}$ mice following a single injection of iron dextran (25 mg/kg body weight) (n=6 mice/group). B. Summary of mean fluorescence intensity (MFI) measured in Calcein-loaded splenic macrophages obtained from iron dextran–injected *Rnf217*$^{flox/flox}$ and *Rnf217*$^{Lysm/Lysm}$ mice (n=3-4 mice/group). C and D. Perl's Prussian blue staining (C) and quantification (D) of spleen and liver sections prepared from iron dextran–injected *Rnf217*$^{flox/flox}$ and *Rnf217*$^{Lysm/Lysm}$ mice (n=4 mice/group). E.

Serum iron and transferrin saturation levels were measured in iron dextran–injected *Rnf217*$^{flox/flox}$ and *Rnf217*$^{Lysm/Lysm}$ mice (n=6 mice/group). F and G. FPN immunohistochemical staining (F) and quantification (G) of spleen and liver sections prepared from iron dextran–injected *Rnf217*$^{flox/flox}$ and *Rnf217*$^{Lysm/Lysm}$ mice (n=4 mice/group). The scale bars in C and F represent 100 μm. **P*<0.05 (Student's *t*-test).

Supplementary Figure 11

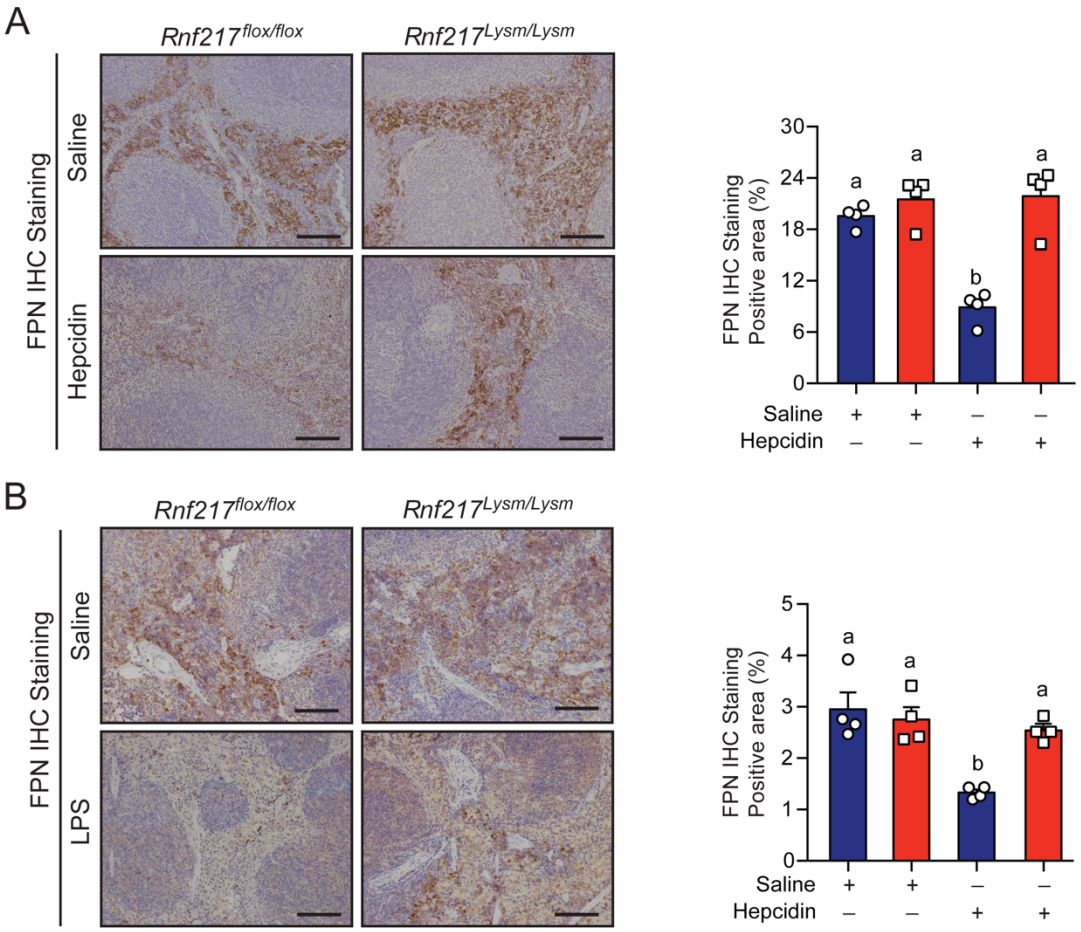

Supplementary Figure S11. RNF217 is involved in hepcidin-mediated FPN degradation *in vivo*. A. FPN immunohistochemical staining and quantification of spleen sections prepared from *Rnf217*$^{flox/flox}$ and *Rnf217*$^{Lysm/Lysm}$ mice injected with either saline or hepcidin (n=4 mice/group). B. FPN immunohistochemical and quantification of spleen sections prepared from *Rnf217*$^{flox/flox}$ and *Rnf217*$^{Lysm/Lysm}$ mice injected with either saline of LPS (n=4 mice/group). The scale bars in A and B represent 100 μm. Groups labeled without a common letter were significantly different (P<0.05; one-way ANOVA).

Supplementary Figure 12

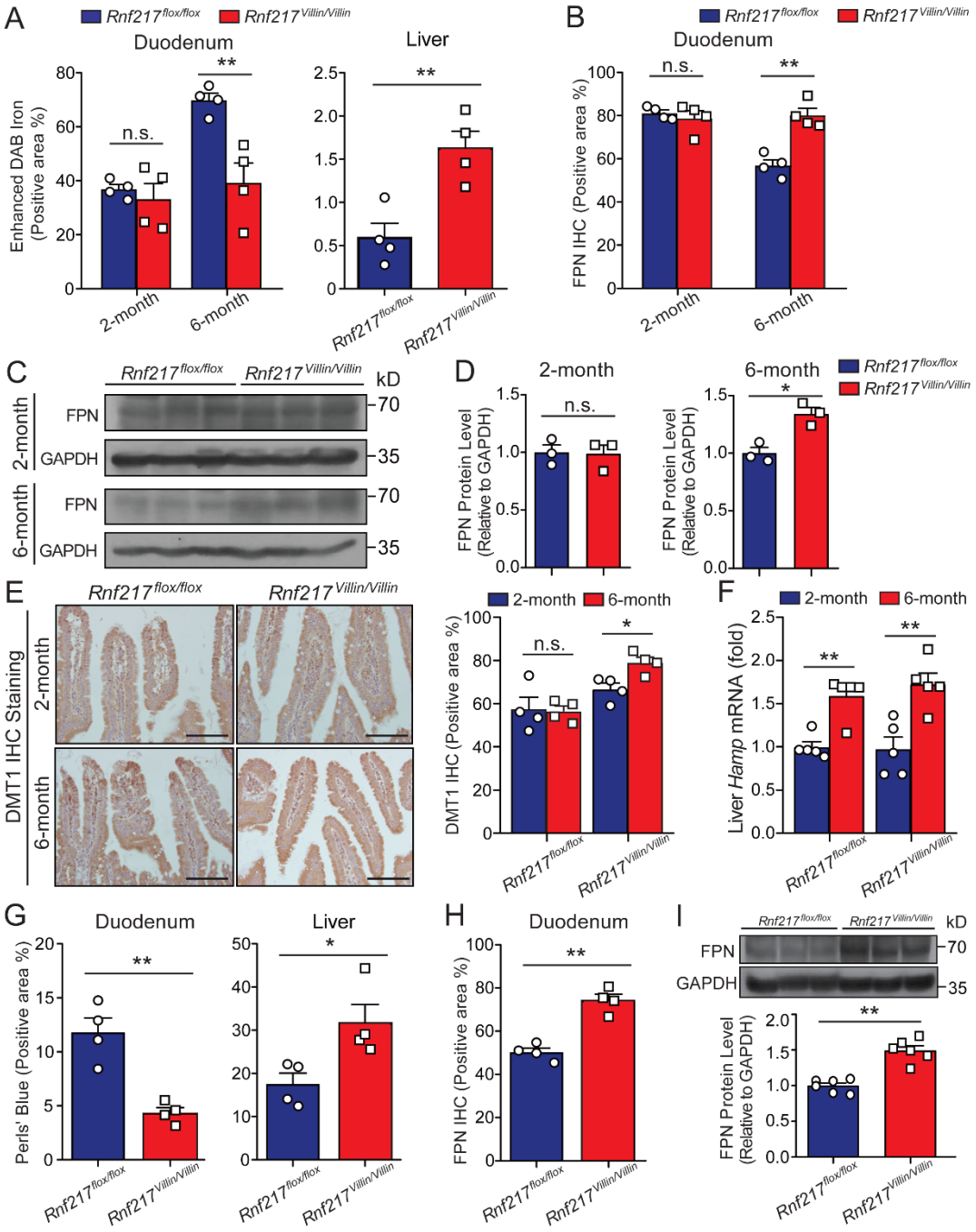

Supplementary Figure S12. Enterocyte-specific *Rnf217* knockout mice increase dietary iron by regulating FPN. A and B. Quantification of enhanced DAB iron staining of duodenum and liver sections (A) and FPN immunohistochemical staining of duodenum sections (B) prepared from *Rnf217*$^{flox/flox}$ and *Rnf217*$^{Villin/Villin}$ mice at the indicated ages (n=4 mice/group). C and D. Western blot analysis (C) and quantification (D) of FPN measured in enterocytes prepared from the small intestinal villi of *Rnf217*$^{flox/flox}$ and *Rnf217*$^{Villin/Villin}$ mice at the indicated ages (n=3 mice/group). E.

Immunohistochemical staining of DMT1 and quantification analysis of duodenum sections prepared from *Rnf217*$^{flox/flox}$ and *Rnf217*$^{Villin/Villin}$ mice at the indicated ages (n=4 mice/group). F. Hepatic *Hamp1* mRNA was measured in *Rnf217*$^{flox/flox}$ and *Rnf217*$^{Villin/Villin}$ mice at the indicated ages (n=5 mice/group). G and H. Quantification of Perl's Prussian blue iron staining of duodenum and liver sections (G), and FPN immunohistochemical staining of duodenum sections (H) obtained from *Rnf217*$^{flox/flox}$ and *Rnf217*$^{Villin/Villin}$ mice fed a high-iron diet for 5 weeks (n=4 mice/group). I. Western blot analysis and quantification of FPN measured in the enterocytes prepared from the small intestinal villi of *Rnf217*$^{flox/flox}$ and *Rnf217*$^{Villin/Villin}$ mice fed a high-iron diet for 5 weeks (n=6 mice/group). The scale bars in E represent 100 μm. **P*<0.05 and ***P*<0.01 (Student's *t*-test).

References

1. Zhang Z, Zhang F, An P, et al. Ferroportin1 deficiency in mouse macrophages impairs iron homeostasis and inflammatory responses. *Blood.* 2011;118(7):1912-1922.
2. Zhang Z, Zhang F, Guo X, An P, Tao Y, Wang F. Ferroportin1 in hepatocytes and macrophages is required for the efficient mobilization of body iron stores in mice. *Hepatology (Baltimore, Md).* 2012;56(3):961-971.
3. Blaschke K, Ebata KT, Karimi MM, et al. Vitamin C induces Tet-dependent DNA demethylation and a blastocyst-like state in ES cells. *Nature.* 2013;500(7461):222-226.
4. Choquet H, Paylakhi S, Kneeland SC, et al. A multiethnic genome-wide association study of primary open-angle glaucoma identifies novel risk loci. *Nat Commun.* 2018;9(1):2278.
5. Thomson JP, Hunter JM, Nestor CE, et al. Comparative analysis of affinity-based 5-hydroxymethylation enrichment techniques. *Nucleic acids research.* 2013;41(22):e206.
6. Dai HQ, Wang BA, Yang L, et al. TET-mediated DNA demethylation controls gastrulation by regulating Lefty-Nodal signalling. *Nature.* 2016;538(7626):528-532.
7. Muto Y, Nishiyama M, Nita A, Moroishi T, Nakayama KI. Essential role of FBXL5-mediated cellular iron homeostasis in maintenance of hematopoietic stem cells. *Nature communications.* 2017;8:16114.
8. Trapnell C, Pachter L, Salzberg SL. TopHat: discovering splice junctions with RNA-Seq. *Bioinformatics.* 2009;25(9):1105-1111.
9. Trapnell C, Roberts A, Goff L, et al. Differential gene and transcript expression analysis of RNA-seq experiments with TopHat and Cufflinks. *Nat Protoc.* 2012;7(3):562-578.
10. Ball MP, Li JB, Gao Y, et al. Targeted and genome-scale strategies reveal gene-body methylation signatures in human cells. *Nat Biotechnol.* 2009;27(4):361-368.

11. Guo JU, Ma DK, Mo H, et al. Neuronal activity modifies the DNA methylation landscape in the adult brain. *Nat Neurosci.* 2011;14(10):1345-1351.

12. Wu H, D'Alessio AC, Ito S, et al. Dual functions of Tet1 in transcriptional regulation in mouse embryonic stem cells. *Nature.* 2011;473(7347):389-393.

13. Williams K, Christensen J, Pedersen MT, et al. TET1 and hydroxymethylcytosine in transcription and DNA methylation fidelity. *Nature.* 2011;473(7347):343-348.

14. Tsai YP, Chen HF, Chen SY, et al. TET1 regulates hypoxia-induced epithelial-mesenchymal transition by acting as a co-activator. *Genome biology.* 2014;15(12):513.

15. Yu C, Zhang YL, Pan WW, et al. CRL4 complex regulates mammalian oocyte survival and reprogramming by activation of TET proteins. *Science (New York, NY).* 2013;342(6165):1518-1521.